# Dosimetry of Microelectrodes Array Chips for Electrophysiological Studies Under Simultaneous Radio Frequency Exposures

Amani Nefzi, Rosa Orlacchio, Lynn Carr, Clement Lemercier, Corinne El Khoueiry, Noelle Lewis, Philippe Lévêque, Delia Arnaud-Cormos

# Dosimetry of Microelectrodes Array Chips for Electrophysiological Studies Under Simultaneous Radiofrequency Exposures

Amani Nefzi, Rosa Orlacchio, Lynn Carr, Clément E. Lemercier, Corinne El Khoueiry, Noëlle Lewis, Philippe Leveque, *Member, IEEE,* Delia Arnaud-Cormos, *Member, IEEE*

***Abstract*— Studying the response of neuronal networks to radiofrequency signals requires the use of a specific device capable of accessing and simultaneously recording neuronal activity during electromagnetic fields (EMF) exposure. In this study, a Microelectrode Array (MEA) that records the spontaneous activity of neurons is coupled to an open transverse electromagnetic (TEM) cell which propagates EMF. We characterize this system both numerically and experimentally at 1.8 GHz. Two MEA versions were compared, for the first time, to determine the impact of their design dissimilarities on the response to EMF. Macroscopic and microscopic measurements using respectively a fiber-optic probe and a temperature-dependent fluorescent dye (Rhodamine-B) were carried out. Results indicate that one MEA shows more stability toward the changes of the surrounding environment compared to the other MEA. Using a fiber-optic thermometer, the measured specific absorption rate (SAR) probe value in the center of the more stable MEA was 5.5±2.3 W/kg. Using a Rhod-B microdosimetry technique, the measured SAR value at the level of the MEA electrodes was 7.0±1.04 W/kg. SAR values are normalized per 1-W incident power. Due to the additional metallic planes and a smaller chip aperture, this new recording chip is steadier in terms of SAR and temperature stability allowing high exposure homogeneity as required during biological experiments. A typical neuronal activity recording under EMF exposure is reported.**

***Index Terms*— Dosimetry, electromagnetic fields (EMFs), microelectrode array (MEA), neuronal network, radiofrequency signals, specific absorption rate (SAR).**

## I. Introduction

THE possibility that electromagnetic fields (EMF) emitted by mobile phones may affect the physiological activity of the central nervous system is one of the most intriguing open matters in bio-electromagnetic research [1]–[3]. The widespread use of portable devices and other wireless communication systems has increased the concern about the risks of possible effects on health, stimulating a large amount of research. Bioelectromagnetic investigations at the cell level of different endpoints were carried out using microsystems exposure systems. For microwave spectrum, microelectrode arrays based on coplanar technology were developed for different electromagnetic diagnostics and therapeutic methods such as dielectrophoresis, dielectric spectroscopy, microfluidics applications [4]–[8]. However, few *in vitro* studies were performed to identify the cellular and molecular mechanisms of the interaction between EMF and neuronal networks. Real-time investigation of electrical activity modifications of neuronal networks, in terms of spiking and bursting rate, under the exposure to low-level radiofrequency (RF) was the object of several studies [9]–[12]. Moreover, the effects induced on neuronal differentiation by millimeter-waves were also investigated [13]. To provide reliable controlled experimental conditions, specific exposure systems were designed. For example, a waveguide or an open Transverse Electromagnetic (TEM) cell for the transmission of the EMF was combined with a microelectrode array (MEA) for the electrophysiological recording of the neuronal activity. The MEA technology was widely used to study *in vitro* the

This paragraph of the first footnote will contain the date on which you submitted your paper for review. This work was supported by ANR Labex SigmaLim, the Region Nouvelle-Aquitaine [grant number AAPR2020A- 2019-8152210] by the French National Research Program for Environmental and Occupational Health of Anses (grant 2015/2 RF/19) and European Union's Horizon 2020 research and innovation program under grant agreement No 737164. (*Corresponding author: Delia Arnaud-Cormos*).

A. Nefzi, R. Orlacchio, and P. Leveque are with the University of Limoges, CNRS, XLIM, UMR 7252, F-87000 Limoges, France (e-mail: amani.nefzi@unilim.fr; rosa.orlacchio@unilim.fr; philippe.leveque@unilim.fr).

L. Carr is with the University of Limoges, CNRS, XLIM, UMR 7252, F-87000 Limoges, France, and also with the School of Electronic Engineer, Bangor University, Bangor, UK (e-mail: lynncarr@gmail.com).

Clément E. Lemercier is with the University of Bordeaux I, CNRS, IMS, UMR 5218 33400 Talence, France, and also with the Ruhr University Bochum, Faculty of Medicine, Department of Systems Neuroscience, Bochum, Germany (e-mail: clement.lemercier@ruhr-uni-bochum.de).

Corinne El Khoueiry and Noëlle Lewis are with the University of Bordeaux I, CNRS, IMS, UMR 5218 33400 Talence, France (e-mail: corinekhoueiry90@hotmail.com; noelle.lewis@u-bordeaux.fr).

D. Arnaud-Cormos is with the University of Limoges, CNRS, XLIM, UMR 7252, F-87000 Limoges, France, and also with the Institut Universitaire de France (IUF), 75005 Paris, France (e-mail: delia.arnaud-cormos@xlim.fr).

spontaneous activity of cultured neural networks or brain slices [14]. This is due to its ability to electrically stimulate neurons at multiple sites and simultaneously measure the extracellular potential changes arising at the cell-electrode interface [14]–[17].

Recording the extracellular potential modifications induced by real-time exposure to RF with an MEA was firstly proposed by Koster *et al*. as a non-invasively alternative to the common patch-clamp technique [9]. In their study, cultured cortical neurons from mice embryos on MEAs, were inserted into a rectangular waveguide for the exposure to continuous wave (CW) or 3G mobile phone signals. Successively, Merla *et al.* designed and characterized a new MEA-based system for electrophysiological recording of neuronal activity during exposure to 1.8 GHz (representative of the Global System for Mobile Communications [GSM] signals), by means of an open TEM cell [10]. A modified device integrating signals acquisition was further used for the analysis of spontaneous bursting activity of primary neuronal cultures from rat embryonic cortices. The neurons were exposed to specific absorption rates (SAR) ranging from 0.01 to 9.2 W/kg [18], [19]. Results showed a dose-dependent reversible decrease in the burst and firing rates of neurons, which is more pronounced as the exposure time and power increase.

More recently, a set-up based on an open TEM cell that accommodates up to six MEA plates was proposed for long-term exposure within a flexible frequency range of mobile telecommunication standards by Oster *et al.* [12]. This device was used to expose neuronal networks at 395 MHz frequency carrier signal, showing no effects on neuronal electrophysiology after long or short exposures to SAR values between 1.17 and 2.21 W/kg [20]. Electrophysiological recordings were performed outside the exposure setup immediately before and after RF exposure and took place between 22 and 34 days in vitro (DIV).

A summary of the studies using an MEA coupled to a specific exposure system is provided, in chronological order, in the Table I. Note that these exposure systems are different in terms of working frequency, source of the EM field, and number of simultaneous MEAs that can be exposed. Briefly, in [9] a single MEA was fitted into a recess of a rectangular waveguide during exposure while in [12] a TEM cell was used to expose up to six MEAs set on the bottom plate of the TEM cell. The exposure system that we proposed in [10] allows the exposure of a single MEA whose holder is inserted in the TEM cell though a circular hole in the ground plate.

Overall, results of these studies suggest that the use of MEAs coupled to an EMF system provides an efficient interface to non-invasively investigate and assess electrophysiological modifications of neuronal activity under RF field exposure. Indeed, an open TEM cell allowed exposure of the samples within the MEAs to 1.8 GHz signals at different input power levels. The latter provides a highly homogeneous *E*-field and was already used by our group combined with a MEA [10].

Since the introduction of the first MEA in 1972 [16], technological efforts have vastly improved the quality of these devices. Improvements include advancements on transducers (microelectrode array, 3D MEA), substrates (active, passive, silicon, CMOS arrays), electrode densities (HD-MEA), mechanical properties (flexible or rigid), and applications (implantable array, *in vivo* MEA, *in vitro* MEA) [14], [21], [22].

TABLE I
OVERVIEW OF THE EXPOSURE SYSTEMS COMBINING AN EM SOURCE AND AN MEA AND THE CORRESPONDING IN VITRO EXPERIMENTS PERFORMED

| Reference | Year | Type of EM source | f (GHz) | *In vitro* experiments |
|---|---|---|---|---|
| [9] | 2007 | Rectangular waveguide | 1.9-2.2 | [9] |
| [10] | 2011 | Open TEM cell | 1.8 | |
| [12] | 2016 | Open TEM cell | DC-1 | [20] |
| Current study | 2021 | Open TEM cell<br>+ MEA-1<br>+ MEA-2 | 1.8<br>1.8 | [18], [19]<br>Ongoing |

In the current study, two different planar MEAs from two different manufacturers QWANE (Qwane, Lausanne, Switzerland) and MCS (Multi Channel Systems MCS, Reutlingen, Germany), were analysed in detail. The first is a customized and modified version of a 60-channel planar MEA introduced in [10]. The contact pads were moved on the lower side of the printed circuit board (PCB) to allow contact underneath the PCB with the preamplifier during RF exposures of neurons. The second device was custom designed to improve the electromagnetic compatibility of the experimental bench, mainly resizing the aperture for optical visualisation and adding ground planes in the multi-layer PCB. This new MEA has never been used for bioelectromagnetic experiments so far, thereby requiring a complete electromagnetic characterization before further recordings of neuronal electrical activity.

Note that to assure precise dosimetry, each exposure system needs to be characterized under the specific exposure conditions of the study, i.e., exposure device, sample exposed and its material, dimensions, position, etc. This means that dosimetry of the MEAs studied here cannot be directly extracted from [10], [23].

Therefore, numerical and experimental dosimetry was carefully carried out to investigate the impact of EMF distribution on the specific MEAs considered in the current study, both at the macro- and micro-scales. In addition to characterize the systems, we analyzed here for the first time the influence of their proximity environment (several different configurations). Also, for the first time, the temperature in the MEAs at the level of the electrodes was measured using a technique optimized by our group to measure the microscopic temperature elevation [23]. The results of this study are essential for future neural activity recordings experiments under 1.8 GHz EMF exposure providing an accurate dosimetry that is crucial for the correct interpretation of potential biological effects.

Section II describes the MEA characteristics, the experimental and numerical dosimetry, and electrophysiology measurements under RF exposure. In Section III, results in terms of electric fields, SAR, temperature, and *in vitro* neural

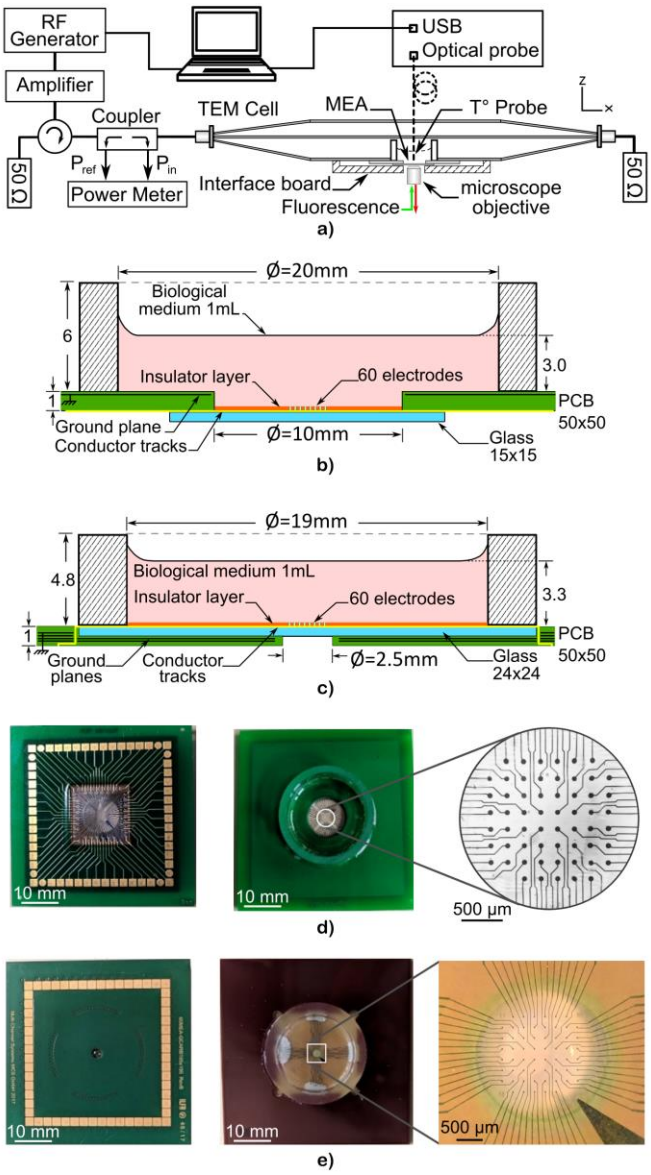


Fig. 1. (a) Setup with the TEM cell exposure device and MEAs for macro- and micro-dosimetry measurements. (b) and (c) 3D CAD models (transversal cut) of MEA-1 and MEA-2, respectively. (d) and (e) Photos (bottom view and top view with a close-up on the electrodes area) of MEA-1 and MEA-2, respectively.

recording measurements for the two MEAs considered are presented. Finally, discussion and conclusions are drawn in Section IV.

## II. Material and Methods

### A. MEA Characteristics

An MEA is a durable and reusable electrophysiology recording device (Fig. 1), allowing the extracellular recording of neural networks activity from various type of brain preparations in a non-invasive manner. The materials used for the fabrication are thoroughly chosen to ensure rigidity, optical transparency, and biocompatibility with the biological samples [1]. An MEA is composed of three parts: i) the culture chamber or well, holding the culture medium, ii) the glass chip, where the electrodes and the top tracks are placed, and iii) the PCB. For the MEAs used in the current study, a glass chip is attached to a 50 mm x 50 mm PCB supporting a glass ring forming the culture chamber. An insulator layer of a few micrometers thickness is set above the tracks leaving the electrodes uncovered to allow the contact with neurons.

The typical MEA design is 60 TiN (indium-tin oxide) or platinum electrodes forming an 8 x 8 matrix situated on the top of a glass chip. Of these electrodes, 59 serve to record the neuronal responses and one as a reference. The electrodes of the MEAs used in this study are designed following a commercial process but using a custom design. The main design particularities of the MEAs are the metal plates inside the PCB, the aperture size, and the inverted position of the preamplifier underneath the PCB. Cultured neurons within the culture chamber adhere to the surface of the MEA in direct contact with the microelectrodes.

In this work, two MEAs (Fig. 1) were dosimetrically characterized, namely MEA-1 of Qwane Biosciences and MEA-2 of MCS companies. The major differences between the two MEAs are: i) the number of metallic planes inside the PCB, ii) the aperture size in the PCB, and iii) the shape of the culture chamber. The metallic planes are represented by the horizontal black lines within the PCBs in Fig. 1 (b) and (c). Specifically, MEA-1 has only one metallic plane in the PCB. The PCB is 1 mm thick, and it has a 10 mm diameter aperture. Its 0.7 mm thick glass chip is attached under the PCB (Fig. 1(b)). MEA-2 has four metallic planes within the PCB, including two at the electrodes and pads levels. The PCB is 1 mm thick, and it has a 2.5 mm diameter aperture. Its 0.5 mm thick glass chip is placed above the PCB (Fig. 1(c)).

### B. Experimental Dosimetry

#### 1) Exposure System

The exposure system consists of a signal generator unit, an amplifier, a circulator, a power meter, and an open TEM cell containing the MEA terminated by a 50 Ω terminator (Fig. 1(a)). The TEM cell was used to apply the *E*-field. It consists of a tri-plates transmission line. The bottom and top metal plates are connected to the reference ground plane, while the middle one, the septum, is the inner conductor. These plates are tapered at their input/output extremities to SMA connectors. The dimensions of the TEM cell were chosen to match 50 Ω impedance. The TEM total length is 160 mm and the length of the central part without the transitions to the SMA connectors is 60 mm. The width of the central septum and of the two external plates is 30 mm and 85 mm, respectively. The distance between the septum and the two external plates is 8 mm (top) and 12 mm (bottom). A 24 mm diameter aperture was made in the bottom plate to insert the MEA. A TEM cell is advantageous because the *E*-field propagating between the plates is homogenous allowing uniform exposure of the biological sample.

An RF signal generator (HP8648B, Hewlett-Packard, USA) was used to generate a CW signal at 1.8 GHz connected to a 44 dB gain amplifier (M.19.40.50, Nuclétudes, France). A bidirectional coupler allows real-time monitoring of incident

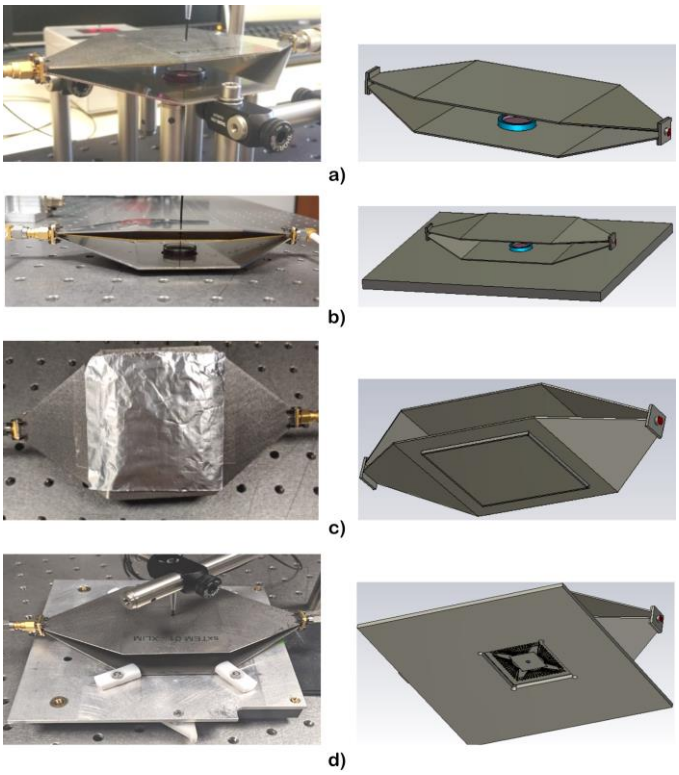


Fig. 2. Photos (on the left) and 3D CAD models (on the right) of the different cases of the exposure system i.e. the TEM cell and the recording device MEA used for experimental and numerical assessments. (a) System suspended in the air (open), (b) system placed on top of a metal plate, (c) system sealed with a metal cavity, and (d) system placed on the preamplifier of the electrophysiological recordings device.

and reflected powers at the TEM cell input through a power-meter (N1912A, Agilent, USA). The TEM cell output port is connected to a 50 Ω terminator that absorbs transmitted power and prevents wave interferences within the device. The MEA is filled with 1 mL of Dulbecco's modified eagle medium (DMEM) culture medium or HEPES buffered salt solution (HBSS).

To fully characterize the system and analyze the influence of its material environment, experiments and simulations were performed under four configurations, combining the TEM cell, the MEA, and their support (Fig. 2): i) suspended in the air above four metal rods, ii) placed above a conductor support, iii) sealed by a metallic cavity, and iv) fixed above the interface board and the signal preamplifier that serves for the electrophysiological recordings. This last configuration is the most representative of the experimental investigation setup. The preamplifier is placed below the MEA to allow the insertion of the culture chamber inside the TEM cell as described in [18], [19]. The preamplifier in the switched OFF state was considered for the SAR dosimetry. Indeed, a slight and slow temperature increase was induced in the sample when the preamplifier was switched ON. However, SAR values are not dependent on the preamplifier state. To evaluate the baseline activity and ensure that exposed and sham conditions represent similar state of temperature increase, a series of sham exposures was carried out separately, using the same protocol

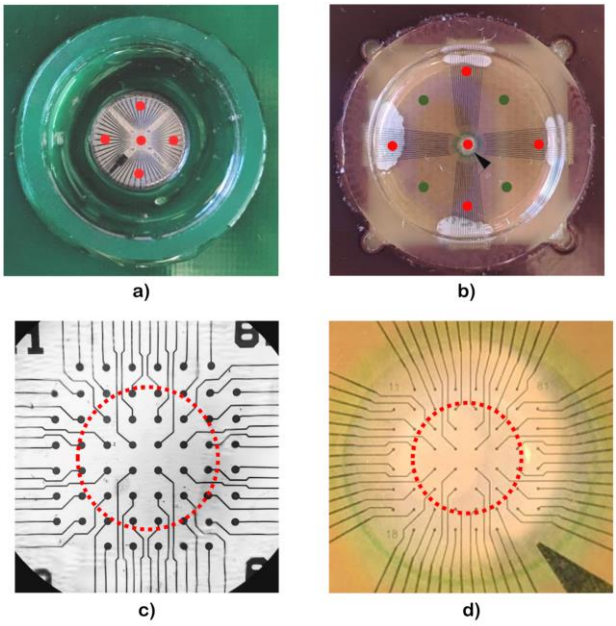


Fig. 3. Top view of the two MEAs. (a) MEA-1 with red dots representing the positions of temperature and fluorescence measurements. (b) MEA-2 with red and green dots for the positions of temperature measurements. Zooms showing the electrodes and the area (dotted line) of temperature evaluation with the FO probe (1 $mm^3$) in (c) MEA-1 and (d) MEA-2.

but with RF always OFF similar to the protocol described in [19]. Moreover, its crucial to consider and avoid possible interferences with external devices. During the experiments, the exposure system was placed in a closed biological incubator whose walls act as a metallic cavity shielding the exposure setup from external interferences. In addition, to reduce interference with the preamplifier, the latter was shielded using a RF absorber.

*2) Macroscale Temperature Measurements*

Macroscale temperature changes in the exposed sample within the MEA chamber were read with a fiber optic (FO) probe (Luxtron One, Lumasense Technologies, CA, USA) inserted through a small hole in the TEM top plate and septum.

We define SAR probe as the SAR extracted from temperature measurements performed with a FO probe immersed in the culture medium, that provides temperature measurements within an estimated 1 $mm^3$ volume. Samples were typically exposed for 1 minute, and temperature was recorded before, during, and after exposure. SAR probe values were extracted from the experimental temperature measurements with:

$$SAR = C \left.\frac{\partial T}{\partial t}\right|_{t = t_0} \quad (1)$$

where $C$ is the specific heat capacity of the biological sample equal to 4186 (J/(kg·K)) and $\partial T/\partial t$ is the initial slope of the temperature increase versus time [24].

Temperature was recorded at different locations within the culture chamber indicated by the dots in Fig. 3(a) and (b).

*3) Microscale Temperature Measurements*

Local microscale temperature change at the level of the electrodes was obtained by exploiting the fluorescent dye Rhodamine-B (Rhod-B) whose fluorescence intensity varies linearly as a function of the temperature [25], [26]. 1 mL of a 50 µM Rhod-B (SigmaAldrich, Saint-Quentin Fallavier, France) solution in HBSS was placed in the MEA microchamber. To acquire real-time fluorescence intensity variation of Rhod-B during the exposure to RF, the MEA attached to the TEM cell, was set on a microscope stage [23]. Rhod-B (excitation: 553 nm, emission: 627 nm) fluorescence intensity was observed by epifluorescence using a solid-state light engine (Spectra 7, Lumencor) coupled to the microscope (DMI6000, Leica). Images were captured on a camera (EMCCD Evolve 512, Roper) with 256 x 256 pixels spatial resolution. Images were collected every second using a 10x microscope objective. Image Analyst MJII (Image Analyst Software, Novato, CA) was used for image analysis. Fluorescence intensity was measured in a 0.32 mm² area (Fig. 4(a) and (b)). Temperature variation retrieved in MEA-1 was assessed in different areas of the device (Fig. 3(a)), while in MEA-2 it was evaluated only in the center (Fig. 3(b)) due to geometrical constraints that did not allow the microscope to reach the peripheric areas. For this configuration, due to technical limitations related to the preamplifier setup on the microscope stage, the preamplifier was not set at the bottom of the MEA. Note that local SAR at the microscopic scale refers to SAR retrieved from Rhodamine-B measurements allowing to consider temperature elevation within a slice with a thickness of tens of microns.

## C. Numerical Modelling

Numerical analysis was performed with the time domain solver of CST Microwave Studio 2017 (Computer Simulation Technology [CST], Dassault Systems, Darmstadt, Germany). All four experimental configurations were modelled and simulated. Metallic components were modelled as Perfect Electric Conductor (PEC). To investigate interferences with the environment, the MEA designs were simplified by disregarding some elements such as electrodes and conductor tracks. For MEA-1, the PCB with the reference metal plane inside, the glass chip, the ring, and the culture medium were simulated. For MEA-2, all the components except the electrodes and the top conductor tracks were simulated.

The dielectric properties of the materials used were modelled at 1.8 GHz. The conductivity ($\sigma$), the relative permittivity ($\varepsilon_r$), and the volume density ($\rho$) of the biological medium were respectively 2.3 S/m, 74.2, and 1000 kg/m$^3$. The neuronal cells and networks were exposed to RF in the MEA chamber filled with classical culture medium. The culture medium dielectric properties considered in simulations were obtained from measurements using a dielectric probe (85070E Dielectric probe kit, Agilent, Santa Clara, CA, USA) connected to the vector network analyzer (the probe tip was inserted in the sample for the measurements). For simulations, we considered a homogenous culture medium sample without cells as classically modelled in *in vitro* studies. The culture chamber and the glass chip were defined as loss free with $\varepsilon_r$ equal to 4.6. The PCB and the layer of insulator covering the top tracks were designed with $\varepsilon_r$ equal to 4.4 and 4, respectively. The culture medium volumes were 1 mL within MEA-1 and MEA-2. In the absence of electrodes, the smallest mesh size considered was 100 µm for accurate results.

The numerical study provides us with the *S* parameters, the *E*-Field spatial distribution inside the TEM cell, and the SAR distribution within the culture medium that is extracted from the electric field through:

$$SAR = \frac{\sigma E^2}{2\rho} \quad (2)$$

where $E$ is the electric field (V/m), $\rho$ is the biological sample density (kg/m$^3$), and $\sigma$ is the electrical conductivity (S/m).

## D. Electrophysiology Under RF Exposure

*1) Primary Cultures of Cortical Neurons*

Primary cortical neuron cultures were prepared from cortices of rat embryos at embryonic day 18, collected from a gestating Sprague-Dawley rat (Charles River Laboratories, L'Arbresle, France). All procedures were carried out in compliance with the European Community Council Directive for the Care and Use of laboratory animals (2010/63/EU). Protocols were approved by the Bordeaux institutional ethics committee (CEEA50). Preparation of primary neural cultures was identical to the method used by [18], [19]. In brief, under anesthesia (5% isoflurane), gestating rats were euthanized (cervical dislocation), embryos were collected, and their cortices were dissected and treated with a papain-based dissociation system (Worthington Biochemical, Lakewood, CO). Following mechanical dissociation and two centrifugation steps (last with an albumin-inhibitor solution), the pellet containing cortical cells (glial cells and neurons) was suspended in a neurobasal culture medium supplemented with 2% B-27, 1% GlutaMAX, and 1% penicillin-streptomycin (Fisher Scientific). Finally, the autoclaved MEAs previously coated with polylysine and laminin (Sigma-Aldrich, St. Quentin-Fallavier, France) were plated with a drop of suspension containing $10^5$ cells. After cell adhesion, MEA wells were filled with culture medium, and kept in individual petri dish at 37°C in a humidified incubator with 5% $CO_2$ until mature neural network development.

*2) Electrophysiological Recording and RF Exposure*

To enable simultaneous recording and exposure to RF, MEAs were maintained sandwiched between the TEM bottom plate and the preamplifier (MEA1060-Inv, Multi-Channel Systems, MCS, Reutlingen, Germany), as described in previous publications [18], [19]. Recordings were performed in a dry incubator at 37 °C with 5% $CO_2$, from 2 cultures at 19 DIV, developed either on MEA-1 or -2. To prevent evaporation while allowing gas exchange throughout the recordings, MEA wells were covered with a thin removable membrane made of fluorinated ethylene propylene (ALA Scientific Instruments, Farmingdale, NY). Preamplification gain was 1200, signals

were acquired and digitized at 10 kHz/channel with an MCS-dedicated data acquisition board (MC_Card, MCS). Signals were recorded and visualized with MC Rack software (MCS).

Neuronal cultures were exposed 15 min to CW signal at 1.8 GHz with an incident power of 5.2 W. In our recordings, this RF-phase was preceded and followed by two 15-min 'control' phases (RF OFF), to compare neuronal spontaneous activity to the activity under RF.

In such electrophysiological experiments, the level of neuronal activity is generally measured by focusing on 'spikes', peaks of dozens of μV that appear out of the noise level. These spikes can arise in an isolated manner or gathered in a dense discharge called 'burst' (Fig. 8).

*3) Data Post-Processing and Analysis*

After recording, multi-channel data processing was performed with the software package SPYCODE [27] developed on MATLAB environment (Mathworks, USA). Following signal filtering (Butterworth high-pass filter with a cutoff frequency at 70 Hz), spike detection was performed with the differential threshold precision timing spike detection (PTSD) method described in [28] and spike trains were then analyzed for bursts detection using the method described in [29]. Burst count were used to compute mean burst rate per minute for each individual channel ($MBR_k$) along all recording phases. The overall behavior of the neural network on the entire MEA was approximated by computing the integral of $MBR_k$ ($MBR_{MEA}$). Change in neural network activity in response to RF exposure was quantified by the ratio between $MBR_{MEA}$ of the exposure phase to the mean $MBR_{MEA}$ of pre-exposure baseline phase. Distribution of spontaneous spike and burst over time was visualized with raster plots created with the software R (R Core Team 2020).

## III. Results

### A. Experimental Macrodosimetry

The SAR probe values retrieved from the experimental temperature measurements within the MEAs (bottom center), for 10 W applied for 5 minutes are presented in Table II as mean ± standard deviation. To ensure the reproducibility of the outcomes, experiments were repeated at least three times per condition, unless stated otherwise. All SAR values are normalized to 1 W incident power. The noteworthy disparity of SAR probe measured within the MEA-1 proves the sensitivity of the device to the surrounding materials. The highest SAR was found when the system is suspended in the air, which considering the standard deviation is close to the SAR value of the preamplifier configuration.

To measure the SAR variability in the culture chamber, the exposure system was suspended above a microscope i.e. the same configuration used to simultaneously measure fluorescence and FO temperature variations within the exposed medium (next sub-section B). Incident power was set to 10 W or 20 W. High incident powers were used to observe a clear and significant temperature elevation (a few degrees) during a short time, required to retrieve the experimental SAR from the initial slope of the temperature elevation. Temperature change and corresponding SAR probe values were measured in different areas (dots in Fig. 3 (a) and (b)) of the culture chamber for both the MEAs. Overall, FO measurement results showed a certain inhomogeneity of the SAR probe values in both devices. For MEA-1, the highest SAR probe of 70.3±13.2 W/kg was observed in the center, i.e. the area above the electrodes. In the left tracks region (Fig. 3(a), left red dot), SAR probe was divided by a 5-fold ratio of the value measured in the center. For MEA-2, the lowest SAR probe of 3.76±0.74 W/kg was measured in the central area containing the electrodes. It increased only by about 1.5 times in the area without the tracks (green dots of Fig. 3(b)). The difference of SAR probe values in the two MEAs centers is consistent with their heating. After 1-minute exposure at 20 W, a temperature variation of 3.2±0.7°C and 0.9±0.2°C were measured in the center of MEA-1 and MEA-2, respectively.

TABLE II
SAR PROBE FROM TEMPERATURE MEASURED AT THE BOTTOM CENTER OF THE MEA PRESENTED AS MEAN ± STANDARD DEVIATION (SAR NORMALIZED PER 1 W INCIDENT POWER)

| | SAR probe (W/kg) | |
|---|---|---|
| Structure environment | MEA-1 | MEA-2 |
| *Open* | 60.7±15.7 | 6.4±1.5 |
| *Metal* | 15.0±3.0 | 3.5±0.5 |
| *Cavity* | 5.2±0.8 | 3.3±0.4 |
| *Preamplifier* | 40.3±5.3 | 5.5±2.3 |

### B. Experimental Microdosimetry

For microdosimetry measurements, Rhod-B fluorescence was recorded with the TEM cell containing the MEAs placed on a microscope stage. To precisely quantify the microscale temperature variation in the exposed sample, it was necessary to establish the relationship between the normalized Rhod-B fluorescence intensity and the temperature measurements from the FO. For small temperature changes, this relationship is linear and a conversion coefficient α can be defined as follows [23]:

$$\alpha = -\frac{\Delta T}{\Delta fluo\,(T)/\Delta fluo\,(0)} \quad (3)$$

where $\Delta T$ is the temperature increment recorded with a FO probe in the solution, and $\Delta fluo\,(T)/\Delta fluo\,(0)$ is the normalized intensity of Rhod-B, i.e., the ratio between the fluorescence value during RFon and the initial fluorescence value at room temperature before RFon. In this study, the conversion coefficient α was equal to –57±2.5, equivalent to a 2%/°C variation of Rhod-B fluorescence, as previously assessed [23], [25], [30], [31].

Following a 1-minute exposure to 20 W, the temperature change in the central area, for both MEAs (Fig. 4(a) and (b)), were calculated from the Rhod-B data (Fig. 4(c) and (d)). Local SAR values, normalized to 1 W, extracted from Rhod-B fluorescence were 159±34.3 W/kg and 7.0±1.04 W/kg, for MEA-1 and MEA-2, respectively. Results obtained at the microscopic level in the area containing the electrodes, reflects a similar behavior as observed at the macroscopic level, with the MEA-1 device having a significantly higher SAR level than

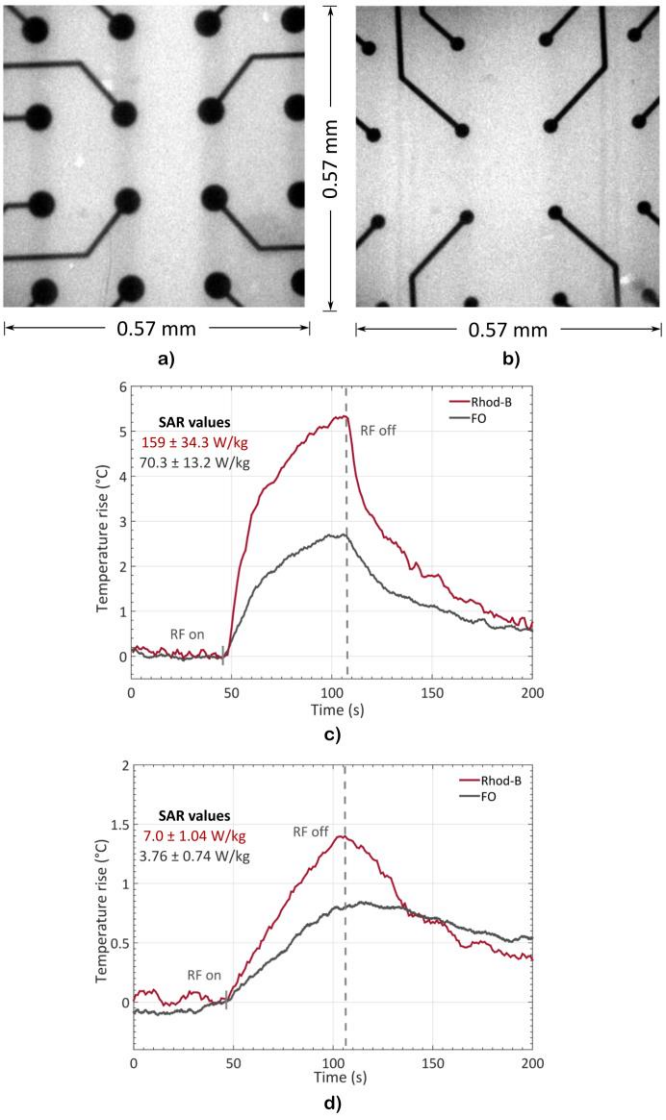


Fig. 4. Microscopic view of the microelectrodes within the 0.57 mm x 0.57 mm area considered for the analysis of Rhod-B in (a) MEA-1 and (b) MEA-2. Temperature dynamics retrieved from Rhod-B (red lines) fluorescence intensity and from the FO thermometer (gray lines), at 20 W of incident power, in (c) MEA-1 and (d) MEA-2.

MEA-2. During these experiments, macroscale temperatures were simultaneously recorded in the same areas with the FO probe (Fig. 4). Macroscale SAR probe values in the central area are equal to 70.3± 13W/kg and 3.76± 0.74 W/kg for the MEA-1 and MEA-2, respectively.

### *C. Numerical Characterization*

Numerical modelling and simulations of the TEM cell, containing simplified designs of the two MEAs were performed for four configurations (open, metal plate, cavity, and preamplifier).

The *E*-field within the TEM cell was analyzed from simulations. The CW signal generated was transformed within the TEM cell into uniform *E*-field with an intensity reversely proportional to the distance between the septum and the external ground plate. For 1 W incident power, the *E*-field

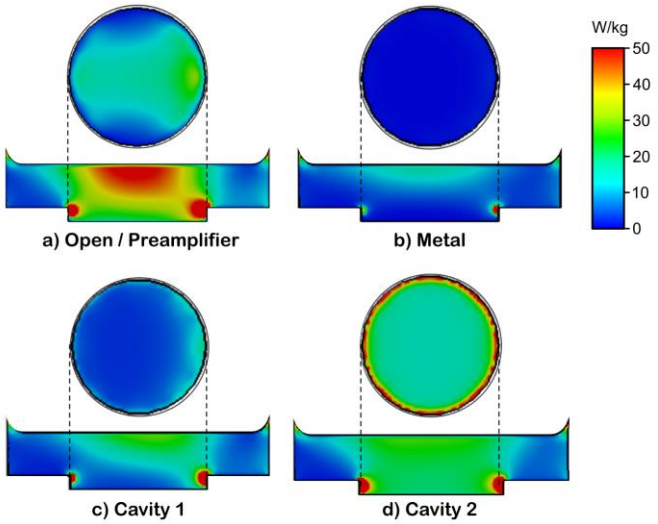


Fig. 5. Numerical SAR spatial distribution at 1.8 GHz of the system (TEM cell & MEA-1), along a horizontal cut at the bottom layer and a vertical cut across the MEA center. (a) System is open (i.e. suspended in the air) or placed above the preamplifier, (b) system placed above a metal plate, (c) system sealed at the bottom with 74 mm x 60 mm metal cavity, and (d) system sealed at the bottom with 60 mm x 60 mm metal cavity.

distribution of the empty TEM cell shows levels around 850 V/m. This is consistent with the theoretical value of 833 V/m calculated for the TEM cell of 12 mm distance between the septum and the lower plate. Thus, creating an aperture in the lower plate to insert the MEA has little effect on the propagation of the TEM mode. However, the *E*-field lines in the vicinity of the hole are distorted as a function of the hole size as illustrated via the SAR distributions with a 36-mm petri dish in [32].

SAR spatial distributions were extracted from simulations for the different studied configurations. Fig. 5 shows the SAR for MEA-1 along a horizontal cut at the bottom layer and a vertical cut across the MEA center. The open and preamplifier configurations (Fig. 5(a)) exhibit similar distributions, which is consistent with measured SAR in the MEA center when considering the standard deviation. Placing the system on a metal plate (Fig. 5(b)), reduces the SAR values. To study the influence of different size metal cavities, Fig. 5(c) and (d) shows the SAR distribution when the system was sealed by a metal cavity with dimensions of either 74 mm x 60 mm or 60 mm x 60 mm. A significant coupling occurs within the 60 mm x 60 mm cavity leading to higher SAR values compared to the 74 mm x 60 mm cavity. This can be explained by the resonance of the smaller cavity. These results demonstrate that the presence of metal around the system influences the SAR values and distribution in MEA-1.

Fig. 6 displays the SAR distribution results for MEA-2. The SAR distributions of all the configurations are almost identical and show good local homogeneity (only two distributions are represented for open/preamplifier and metal/cavities). These results indicate that MEA-2 is more isolated, due to the four metallic planes in the PCB and its smaller chip aperture, and therefore less influenced by the surrounding environment than MEA-1.

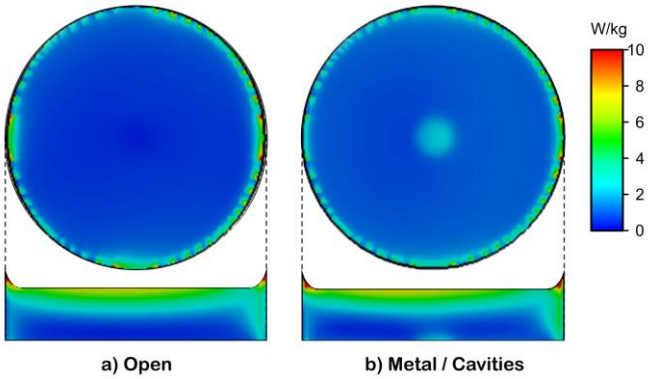


Fig. 6. Numerical SAR spatial distribution at 1.8 GHz in the culture medium within the MEA-2 along a horizontal cut at the bottom layer and a vertical cut across the MEA center. (a) System is above open/preamplifier, and b) system is above metal or sealed with a cavity.

The numerical SAR probe values calculated at the center and the bottom of the medium within a 1 $mm^3$ volume are presented in Table III for the two MEAs. Similar values were obtained for the open and preamplifier configurations for both MEAs. The efficiencies and the standard deviations presented in Table III show the stability of MEA-2. For the non-metal environment, the SAR is around 0.48±0.27 W/kg while with the metal cases it ranges between 1.27±0.34 W/kg and 1.44±0.38 W/kg. The standard deviation illustrates the SAR variation along the height of the culture medium. However, this variation is not critical in relation to the electrodes level where the neurons are exposed. Adding a metal under MEA-2, slightly rises the efficiency at the bottom center of the medium where the PCB aperture is placed.

To assess the influence of electrodes and tracks, numerical microdosimetry was performed on MEA-2. To integrate the electrodes and the tracks in the modelling, a compact TEM cell was designed with 970 µm distance between the septum and the lower plate. A ratio of 12.3 between the initial and compact TEM cells is applied. The biological medium was reduced to 1.9 µL. In the modelling, the electrodes were designed with a 30 µm diameter and a 50 µm height. The meshing of the electrodes was set to be 2 x 2 µm along the electrodes' diameter and 10 µm along the height. Fig. 7 shows the *E*-field distribution at the level of the electrodes for a 1.8 GHz exposure displayed along a horizontal cut at the top surface of the electrodes. Neurons are however mainly located between the MEA electrodes where the *E*-field and consequently the SAR are rather homogeneous. Therefore, the whole SAR volume averaged over the biological sample volume and the SAR probe are only slightly influenced by the presence of the electrodes.

### *D. Biological Characterization*

The two systems were then compared in terms of neuronal cultures development and recording, with or without RF exposure. Fig. 8 shows different representations of the neuronal network electrical activity, recorded in MEA-1 or MEA-2. Cultures are recorded at the same age DIV19. For readability reasons, 10 channels among the 60 were chosen (Fig. 8(a)). The raster plots (Fig. 8(b), (c), (d)) present in a synthetic view 3 min

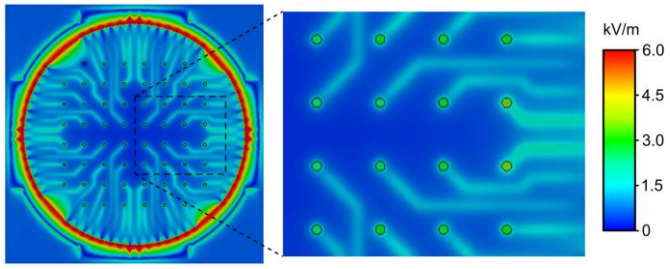


Fig. 7. Numerical electric field spatial distribution at 1.8 GHz of MEA-2 within a micro-TEM cell; the distribution is plotted in the culture medium along a horizontal cut at the top surface of the electrodes.

TABLE III
SIMULATED SAR PROBE PRESENTED AS MEAN ± STANDARD DEVIATION (FOR 1 W INCIDENT POWER)

| | SAR (W/kg) | |
|---|---|---|
| | MEA-1 | MEA-2 |
| *Open/Preamplifier* | 24.3±5.7 | 0.48±0.27 |
| *Metal* | 0.85±0.53 | 1.27±0.34 |
| *Cavity1 (74x60 mm)* | 5.0±1.6 | 1.44±0.38 |
| *Cavity2 (60x60 mm)* | 19.0±3.1 | 1.42±0.40 |

of electrical activity where spike events appear as little vertical segments.

The two MEAs showed similar activity profiles with balanced activity between isolated spikes and bursts (Fig. 8(b), (c)) suggesting an equivalent level of culture maturation [33], [34]. In comparison to MEA-1, MEA-2 exhibited lower noise level and improved signal to noise ratio.

The ability of MEA-1 and MEA-2 to record neuronal activity under RF was explored successfully. We present here preliminary measurements with MEA-2. RF incident power was set at 5.2 W and 15 min of exposure at this power resulted in an increase of approximately 1 °C of the culture medium. Typical electrical activity recorded from MEA-2 in control condition (RF OFF) is shown in Fig. 8(c) (10 channels over 3 min and a zoom of about 20 sec on electrode 44). The same representation is given to illustrate the exposed phase (RF ON). Previously [18], [19], with MEA-1, we could observe that cultures of cortical neurons are sensitive to RF and exhibit an inhibitory response being more pronounced as the exposure time and power increase.

Although Fig. 8(d) zoom only gives a qualitative view of a sparser bursting activity, RF exposure also inhibited neural network activity of cultures developed on MEA-2. Analyzed over the whole MEA, burst distribution under RF decreased (42.4% reduction in $MBR_{MEA}$ relative to baseline) whereas the rate of isolated spikes (outside bursts) was less affected (4.5% reduction in frequency rate relative to baseline).

However, considering the SAR probe value of MEA-2, a SAR of 28.6 W/kg is assessed for these experiments. This SAR value is significantly higher than the local basic restriction for RF exposure [35]. Therefore, further investigations should be carried out to study these responses at different SAR levels.

Together these observations made in real conditions validate MEA-2 for the culture of neural networks and for their electrophysiological monitoring with or without continuous RF exposure.

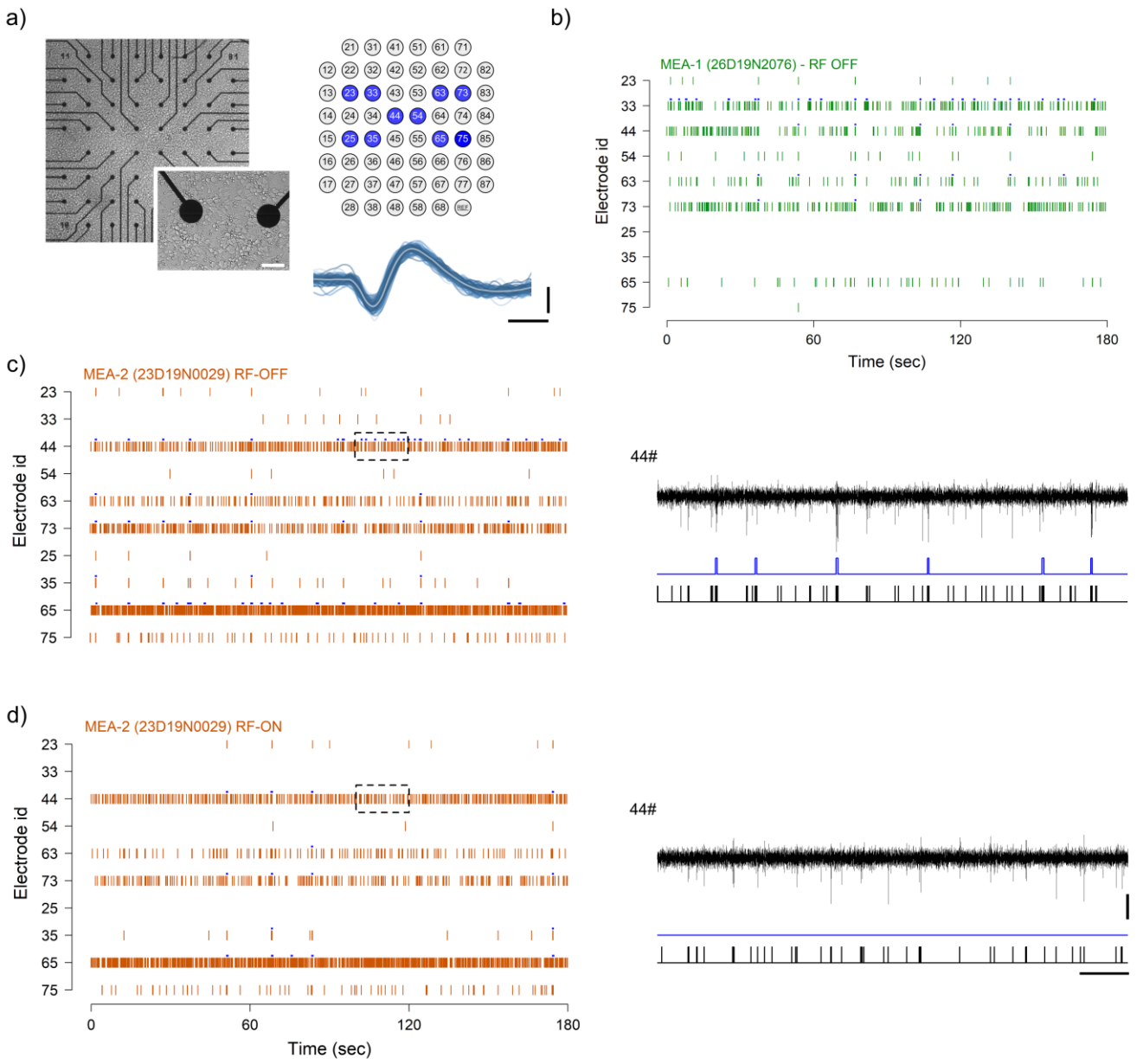


Fig. 8. Recording of cortical neural networks electrical activity. (a) Bright-field microscopy images showing a culture of cortical neurons plated on MEA-2; higher magnification picture showing two electrodes surrounded by neural cell bodies (scale bar: 30 µm); superimposition of 100 single-unit spike waveforms, in gray is the average spike waveform (scale: (y): 40 µV; (x): 0.5 msec); illustration showing the relative position within the MEA of the 10 selected channels showed individually in panels b), c), and d). (b-c) Raster-plot from the 10 selected channels showing the spontaneous occurrence of spikes and bursts over three minutes of recording from two cultures at the same age (DIV19, RF-OFF) developed either on (b) MEA-1 and (c) MEA-2, blue markers indicate bursting activity. (d) Raster-plot from the same culture shown in (c) under continuous exposure to RF (RF-ON, CW 5.2 W). Right to (c-d) is shown the corresponding electrical activity from a single electrode (#44) respectively under RF-OFF and -ON exposure (scale: (y): 30 µV; (x): 2 sec).

## IV. Discussion and Conclusion

In this study, we have characterized numerically and experimentally at 1.8 GHz, two real-time exposure systems based on an open TEM cell containing modified or novel MEA recording chips. To analyze the influence of the systems local environments, several positioning conditions were carefully analyzed: above air, a metallic support, a cavity, or a preamplifier. These two MEA systems were characterized in experimental conditions that best approximate conditions employed in electrophysiological experiences [18], [19]. Overall, these measurements are essential to define a reference for the final biomedical setup able to expose neuronal network to RF and simultaneously record their activity under controlled EM and thermal conditions.

Based on an accurate dosimetric study, both MEAs can be used for neuronal recordings under RF exposure. However, MEA-1 shows a stronger sensitivity to its environment than MEA-2, which has a smaller aperture and contains four metal

plates within the PCB. More precisely, the numerical and experimental studies allowed to analyze and evidence the contribution of MEAs different components on the SAR values and stability. The glass chip thickness and the preamplifier presence showed negligible contribution. On the contrary, the presence of the glass ring, the PCB, or the culture chamber volume showed relevant contribution of about 10% variation on the SAR. Finally, a significant contribution (higher than 25%) was due to the aperture in the PCB, the ground planes, and the proximity environment, particularly for a large aperture size. Numerical simulations allowed extracting the SAR distributions within the MEAs at different scales. Note, that SAR is affected by the sample properties. However, biological cells have not been modelled in our case due to their microscopic size and to the fact they do not significantly influence macroscopic properties of the biological medium. Therefore, the difference between the SAR probe values of the two MEAs is due to variation in the geometry and composition of the devices and how they are affected by their environment.

Experimental macrodosimetry and microdosimetry were performed through temperature measurements with a FO thermometer and the fluorescent temperature dependent dye Rhod-B, respectively. The ratio of local heating values between macroscopic (FO) and microscopic (Rhod-B) measurements was approximately 2 after 1-minute exposure. This ratio can be explained by the different measurement volume: i.e. 1 $mm^3$ for the FO probe and a slice with a thickness of a few tens of microns for Rhod-B. Note that SAR may slightly vary along the height of the culture medium with peak SAR observed in proximity of the electrodes tips. However, Rhod-B images measurements acquired in the plane containing the electrodes, where the neurons are exposed, evidence a homogeneous temperature variation without local hot spots. The measured SAR probe values in the center of the MEAs placed above the preamplifier were 40.3±5.3 W/kg and 5.5±2.3 W/kg for MEA-1 and MEA-2, respectively. The measured SAR value for MEA-2 with the Rhod-B microdosimetry technique at the level of the neuronal cells was 7.0±1.04 W/kg.

In conclusion, our results showed that the MEA-2 recording chip is steadier in terms of SAR and temperature stability within the exposed area, representing a better device for future experiments involving electrophysiological recording of neuronal activities. Electrophysiological neural activity recordings with the studied MEAs were performed at SAR levels higher than 25 W/kg and the complete and detailed biological results are in the process of submission in a journal of biology.

## ACKNOWLEDGMENT

The authors would like to thank Clemens Boucsein (Multi Channel Systems MCS, Reutlingen, Germany) and Marc Heuschkel (Qwane Biosciences, Lausanne, Switzerland) for MEA design and their assistance with MEA information for numerical modeling.

## REFERENCES

[1] M. N. Halgamuge, E. Skafidas, and D. Davis, ‘A meta-analysis of in vitro exposures to weak radiofrequency radiation exposure from mobile phones (1990–2015)’, *Environmental Research*, p. 109227, Feb. 2020.

[2] J. Lameth, D. Arnaud-Cormos, P. Lévêque, S. Boillée, J.-M. Edeline, and M. Mallat, ‘Effects of a Single Head Exposure to GSM-1800 MHz Signals on the Transcriptome Profile in the Rat Cerebral Cortex: Enhanced Gene Responses Under Proinflammatory Conditions’, *Neurotoxicity Research*, vol. 38, no. 1, pp. 105–123, Jun. 2020.

[3] D. H. Gultekin and P. H. Siegel, ‘Absorption of 5G Radiation in Brain Tissue as a Function of Frequency, Power and Time’, *IEEE Access*, vol. 8, pp. 115593–115612, 2020.

[4] D. Havelka, O. Krivosudský, and M. Cifra, ‘Grounded coplanar waveguide-based 0.5–50 GHz sensor for dielectric spectroscopy’, in *2017 47th European Microwave Conference (EuMC)*, Oct. 2017, pp. 950–953. doi: 10.23919/EuMC.2017.8231003.

[5] S. Afshar, E. Salimi, K. Braasch, M. Butler, D. J. Thomson, and G. E. Bridges, ‘Multi-frequency DEP cytometer employing a microwave sensor for dielectric analysis of single cells’, *IEEE Transactions on Microwave Theory and Techniques*, vol. 64, no. 3, pp. 991–998, Mar. 2016.

[6] K. Grenier *et al.*, ‘Recent advances in microwave-based dielectric spectroscopy at the cellular level for cancer investigations’, *IEEE Transactions on Microwave Theory and Techniques*, vol. 61, no. 5, pp. 2023–2030, May 2013.

[7] X. Ma *et al.*, ‘A multistate single-connection calibration for microwave microfluidics’, *IEEE Transactions on Microwave Theory and Techniques*, vol. 66, no. 2, pp. 1099–1107, Feb. 2018.

[8] Y. Ning *et al.*, ‘Broadband electrical detection of individual biological cells’, *IEEE Transactions on Microwave Theory and Techniques*, vol. 62, no. 9, pp. 1905–1911, Sep. 2014.

[9] P. Koester, J. Sakowski, W. Baumann, H.-W. Glock, and J. Gimsa, ‘A new exposure system for the in vitro detection of GHz field effects on neuronal networks’, *Bioelectrochemistry*, vol. 70, no. 1, pp. 104–114, Jan. 2007.

[10] C. Merla, N. Ticaud, D. Arnaud-Cormos, B. Veyret, and P. Leveque, ‘Real-time RF exposure setup based on a multiple electrode array (MEA) for electrophysiological recording of neuronal networks’, *IEEE Transactions on Microwave Theory and Techniques*, vol. 59, no. 3, pp. 755–762, Mar. 2011.

[11] A. W. Daus, M. Goldhammer, P. G. Layer, and C. Thielemann, ‘Electromagnetic exposure of scaffold-free three-dimensional cell culture systems’, *Bioelectromagnetics*, vol. 32, no. 5, pp. 351–359, 2011.

[12] S. Oster, A. W. Daus, C. Erbes, M. Goldhammer, U. Bochtler, and C. Thielemann, ‘Long-term electromagnetic exposure of developing neuronal networks: A flexible experimental setup.’, *Bioelectromagnetics*, vol. 37, no. 4, pp. 264–278, Apr. 2016.

[13] A. J. Haas, Y. Le Page, M. Zhadobov, R. Sauleau, and Y. Le Dréan, ‘Effects of 60-GHz millimeter waves on neurite outgrowth in PC12 cells using high-content screening’, *Neuroscience Letters*, vol. 618, pp. 58–65, Apr. 2016, doi: 10.1016/j.neulet.2016.02.038.

[14] M. E. J. Obien, K. Deligkaris, T. Bullmann, D. J. Bakkum, and U. Frey, ‘Revealing neuronal function through microelectrode array recordings’, *Front Neurosci*, vol. 8, Jan. 2015.

[15] U. Egert, D. Heck, and A. Aertsen, ‘Two-dimensional monitoring of spiking networks in acute brain slices’, *Exp Brain Res*, vol. 142, no. 2, pp. 268–274, Jan. 2002.

[16] C. A. Thomas, P. A. Springer, G. E. Loeb, Y. Berwald-Netter, and L. M. Okun, ‘A miniature microelectrode array to monitor the bioelectric activity of cultured cells’, *Experimental Cell Research*, vol. 74, no. 1, pp. 61–66, Sep. 1972.

[17] M. E. Spira and A. Hai, ‘Multi-electrode array technologies for neuroscience and cardiology’, *Nature Nanotech*, vol. 8, no. 2, pp. 83–94, Feb. 2013.

[18] D. Moretti *et al.*, ‘In-vitro exposure of neuronal networks to the GSM-1800 signal’, *Bioelectromagnetics*, vol. 34, no. 8, pp. 571–578, 2013.

[19] C. El Khoueiry *et al.*, ‘Decreased spontaneous electrical activity in neuronal networks exposed to radiofrequency 1,800 MHz signals’, *Journal of Neurophysiology*, vol. 120, no. 6, pp. 2719–2729, Aug. 2018.

[20] T. Köhler, M. Wölfel, M. Ciba, U. Bochtler, and C. Thielemann, ‘Terrestrial Trunked Radio (TETRA) exposure of neuronal in vitro networks’, *Environmental Research*, vol. 162, pp. 1–7, Apr. 2018.

[21] R. Kim, S. Joo, H. Jung, N. Hong, and Y. Nam, 'Recent trends in microelectrode array technology for in vitro neural interface platform', *Biomed. Eng. Lett.*, vol. 4, no. 2, pp. 129–141, Jun. 2014, doi: 10.1007/s13534-014-0130-6.

[22] M. Chiappalone, V. Pasquale, and M. Frega, Eds., *In Vitro Neuronal Networks: From Culturing Methods to Neuro-Technological Applications*. Springer International Publishing, 2019. doi: 10.1007/978-3-030-11135-9.

[23] A. Nefzi, L. Carr, C. Dalmay, A. Pothier, P. Leveque, and D. Arnaud-Cormos, 'Microdosimetry using Rhodamine B within macro- and microsystems for radiofrequency signals exposures of biological samples', *IEEE Transactions on Microwave Theory and Techniques*, pp. 1–9, 2019.

[24] IEEE, 'IEEE Recommended Practice for Determining the Peak Spatial-Average Specific Absorption Rate (SAR) in the Human Head from Wireless Communications Devices: Measurement Techniques', *IEEE Std 1528-2013 (Revision of IEEE Std 1528-2003)*, pp. 1–246, Sep. 2013.

[25] D. Ross, M. Gaitan, and L. E. Locascio, 'Temperature measurement in microfluidic systems using a temperature-dependent fluorescent dye', *Anal. Chem.*, vol. 73, no. 17, pp. 4117–4123, Sep. 2001.

[26] Y. Y. Chen and A. W. Wood, 'Application of a temperature-dependent fluorescent dye (Rhodamine B) to the measurement of radiofrequency radiation-induced temperature changes in biological samples', *Bioelectromagnetics*, vol. 30, no. 7, pp. 583–590, 2009.

[27] L. L. Bologna *et al.*, 'Investigating neuronal activity by SPYCODE multi-channel data analyzer', *Neural Netw*, vol. 23, no. 6, pp. 685–697, Aug. 2010, doi: 10.1016/j.neunet.2010.05.002.

[28] A. Maccione, M. Gandolfo, P. Massobrio, A. Novellino, S. Martinoia, and M. Chiappalone, 'A novel algorithm for precise identification of spikes in extracellularly recorded neuronal signals', *Journal of Neuroscience Methods*, vol. 177, no. 1, pp. 241–249, Feb. 2009.

[29] V. Pasquale, S. Martinoia, and M. Chiappalone, 'A self-adapting approach for the detection of bursts and network bursts in neuronal cultures', *J Comput Neurosci*, vol. 29, no. 1, pp. 213–229, Aug. 2010.

[30] R. Fu, B. Xu, and D. Li, 'Study of the temperature field in microchannels of a PDMS chip with embedded local heater using temperature-dependent fluorescent dye', *International Journal of Thermal Sciences*, vol. 45, no. 9, pp. 841–847, 2006, doi: https://doi.org/10.1016/j.ijthermalsci.2005.11.009.

[31] R. Samy, T. Glawdel, and C. L. Ren, 'Method for Microfluidic Whole-Chip Temperature Measurement Using Thin-Film Poly(dimethylsiloxane)/Rhodamine B', *Anal. Chem.*, vol. 80, no. 2, pp. 369–375, Jan. 2008, doi: 10.1021/ac071268c.

[32] M. Soueid *et al.*, 'Electromagnetic Analysis of an Aperture Modified TEM Cell Including an Ito Layer for Real-Time Observation of Biological Cells Exposed to Microwaves', *Progress In Electromagnetics Research*, vol. 149, pp. 193–204, 2014, doi: 10.2528/PIER14053108.

[33] J. van Pelt, P. S. Wolters, M. A. Corner, W. L. C. Rutten, and G. J. A. Ramakers, 'Long-term characterization of firing dynamics of spontaneous bursts in cultured neural networks', *IEEE Trans Biomed Eng*, vol. 51, no. 11, pp. 2051–2062, Nov. 2004.

[34] D. A. Wagenaar, J. Pine, and S. M. Potter, 'An extremely rich repertoire of bursting patterns during the development of cortical cultures', *BMC Neurosci*, vol. 7, p. 11, Feb. 2006.

[35] ICNIRP, 'Guidelines for Limiting Exposure to Electromagnetic Fields (100 kHz to 300 GHz)', *Health Physics*, vol. 118, no. 5, pp. 483–524, May 2020, doi: 10.1097/HP.0000000000001210.

**Amani Nefzi** was born in Tunis, Tunisia, in 1993. She received the master's degree in electronics from the University of Limoges, Limoges, France, in 2017, where she is currently pursuing the Ph.D. degree in electronics engineering at National Center of Scientific Research (CNRS), XLIM Research Institute. Her current research interests include the development of electromagnetic and nanosecond pulsed electric fields exposure systems for the study of the health and therapeutic effects.

**Rosa Orlacchio** was born in Sapri, Italy. She received the M.Sc. degree in Biomedical Engineering, (with honours), from "La Sapienza", University of Rome, Roma, Italy, and the Ph.D degree in Bio-electromagnetics from the Institute of Electronics and Telecommunications of Rennes (IETR), University of Rennes 1, Rennes, France, in 2014 and 2019, respectively. She is currently a Postdoctoral Researcher with the Bioelectromagnetics Team, XLIM Research Institute, CNRS, University of Limoges, Limoges, France. Her current research interests include the evaluation of the biological effects of nanosecond pulses on cells, and thermal electromagnetic dosimetry and microdosimetry.

**Lynn Carr** received the B.Sc. degree (Hons) in biochemistry from University College London, London, U.K., and the master's degree in biotechnology and the Ph.D. degree from the University of Limoges, Limoges, France. As part of the XLIM Research Institute's BioEM Group, her interests focus on the effects of nanosecond pulsed electric fields on cancer cells with a particular focus on cell signaling.

**Clément E. Lemercier** was born in Rouen, France, in 1990. He received the Ph.D. degree in neurobiology from the Humboldt University of Berlin, Germany in 2018. Between 2018 and 2019, he joined the research group BioEM at IMS lab in Bordeaux and carried out experiments combining electrophysiology and pharmacology to disentangle putative biological mechanisms of the non-thermal effects of radiofrequency electromagnetic fields on cortical neural networks. He is currently a postdoctoral researcher at the Department of systems neuroscience at the Ruhr University Bochum, Germany. His current research focuses on mice audiovisual information processing with electrophysiology and optical imaging technics.

**Corinne El Khoueiry** was born in Beirut, Lebanon, in 1990. She received the Ph.D. degree in neuroscience from the University of Auvergne, Clermont-Ferrand, France. She joined the BioEM team at IMS lab from 2015 until 2018 and worked on the MOTUS project focusing on the study of the effects of radiofrequency field on the activity of neuronal networks in vitro and in vivo. She is currently a postdoctoral researcher in the Center for Psychiatric Neurosciences of the university hospital (CHUV) in Lausanne, Switzerland. Her current research interests include the study of the thalamic circuitry in a mouse model relevant to schizophrenia.

**Noëlle Lewis** (M'09) received the Ph.D degree in electrical engineering from the University of Bordeaux, Bordeaux, France, in 1997. In 2000, she was appointed Assistant Professor in the IMS laboratory at the University of Bordeaux, where she carried out research in analog and mixed circuits design, behavioral modeling, and design automation. In 2005, she joined the research team in engineering of neuromorphic systems to contribute to solve some critical points related to analog integration with IP reuse techniques. In 2010, she was the head of a new research team focusing on electronics interfacing biology (ELIBIO), in which three permanent researchers, two engineers and three doctoral students were involved. She has been a Full Professor since 2013. Her main research interests are front-end circuits for biomedical applications, bio-signal acquisition, and electrical stimulation; the biophysical interaction and its characterization at the tissue-electrode interface. Since 2016 she is the head of the Bioelectronics department at IMS lab, a pluridisciplinary department whose research projects lie at the interface of physics, electronics, biology and medicine.

**Philippe Leveque** (M'03) was born in Poitiers, France, in 1964. He received the Ph.D. degree from the University of Limoges, Limoges, France, in 1994. In 1995, he joined C.N.R.S. He is involved in the development of dosimetry and exposure setups for health-risk assessment in cooperation with biological and medical research groups. He is currently a Senior Scientist with CNRS and the Group Leader of Bioelectromagnetics Team with the XLIM Research Institute focusing on nanopulse application. His current research interest includes the scattering problems of electromagnetic waves, particularly in the time domain.

**Delia Arnaud-Cormos** (M'05) was born in Cugir, Romania, in 1978. She received the Diplôme d'Ingénieur degree from the Institute of Computer Science and Communication, Rennes, France, in 2002, and the master's and Ph.D. degrees from INSA, Rennes, in 2003 and 2006, respectively. Since 2007, she has been with the Bioelectromagnetics Team, XLIM Institute, University of Limoges/C.N.R.S., Limoges, France, as an Associate Professor. In 2012, she joined the Pulsed Power Group, University of Southern California (USC), Los Angeles, SC, USA, where she developed research with the Biological Applications Research Team. Since 2018, she has been a Junior Member with the Institut Universitaire de France (IUF), Paris, France, and a member of the International Bioelectrics Consortium. Her current research interests include nanosecond pulses/microwave exposure system setup and dosimetric characterization for bioelectromagnetic studies.